ACS APPLIED ELECTRONIC MATERIALS

pubs.acs.org/acsaelm Article

Boosting the Performance of One-Step Solution-Processed Perovskite Solar Cells Using a Natural Monoterpene Alcohol as a Green Solvent Additive

Giuliana Giuliano, Aurelio Bonasera, Michelangelo Scopelliti, Delia Chillura Martino, Tiziana Fiore, and Bruno Pignataro*

Cite This: *ACS Appl. Electron. Mater.* 2021, 3, 1813−1825 Read Online

ACCESS | Metrics & More | Article Recommendations | Supporting Information

ABSTRACT: The perovskite film is the core of a perovskite solar cell (PSC), and its quality is crucial for the performance of such devices. The morphology, crystallinity, and surface coverage of the perovskite layer greatly affect the power conversion efficiency (PCE), hysteresis, and long-term stability of PSCs. The incorporation of appropriate solvent additives in the perovskite precursor solution is an effective strategy to control the film morphology and reduce the defects and grain boundaries. However, the commonly used solvent additives are environmentally harmful and highly toxic. In this work, α-terpineol (a nontoxic, eco-friendly, and low-cost monoterpene alcohol) is employed for the first time as an alternative green solvent additive to improve the quality of one-step solution-processed $CH_3NH_3PbI_{3-x}Cl_x$ films and to restrain nonradiative recombination in the corresponding devices. An in-depth investigation of the physicochemical effects induced by such a high-boiling-point, polar protic solvent when incorporated into a conventional perovskite solvent system is provided. The collected data demonstrate that the addition of a precise amount of α-terpineol can generate uniform and highly crystalline perovskite films with improved photovoltaic performances. Through this approach, the PCE of planar n−i−p PSCs is boosted up to 17.5% (against 16.1% of the top control device) with reduced hysteresis and enhanced ambient stability.

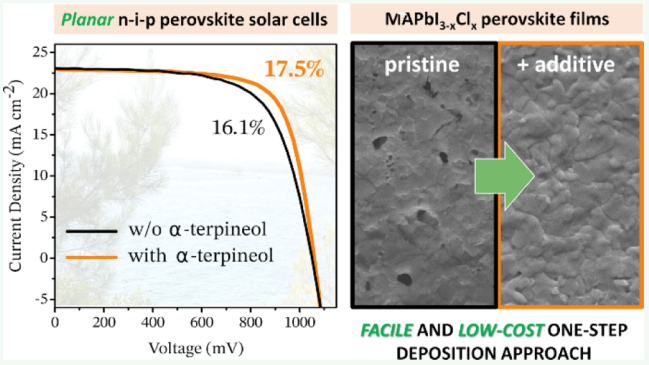

KEYWORDS: *perovskite solar cells, additives, solvent engineering, terpineol, alcohol, green, one-step deposition*

1. INTRODUCTION

Organic−inorganic hybrid perovskite solar cells (PSCs) have drawn tremendous research interest during the last decade since they have emerged as one of the most standout photovoltaic (PV) technologies in terms of performance, with the record certified cell efficiency having recently reached 25.5%.[1−4] PSC devices are exceptional in the way they exhibit extraordinary power conversion efficiencies (PCEs) while utilizing inexpensive fabrication processes and introducing appealing additional features such as flexibility and semi-transparency.[5−7] Despite the astonishing progress achieved in the last few years, the PSC technology is still facing some critical issues regarding the operation, composition, and stability of the devices that need to be addressed before mass production.[2] At present, one of the main challenges is the control of perovskite film formation and crystallization. It is well known that poor perovskite morphology/crystallinity can limit the efficiency of charge dissociation, transport, and collection in the devices.[8] In particular, a high concentration of defects and grain boundaries in the perovskite layer creates severe shorting and trapping sites for nonradiative charge recombination, which is recognized as one of the main causes of PCE losses in PSCs.[9] Defect- and grain-boundary-assisted charge recombination is also related to anomalous hysteresis phenomena and long-term stability issues.[10,11] Therefore, optimizing the perovskite layer by passivating the defects and improving the film quality has become an important strategy to reduce recombination losses, remove adverse hysteresis, prolong the device lifetime, and boost PCE toward the theoretical Shockley−Queisser (SQ) limit.[12,13]

To date, several deposition methods have been developed, aiming to achieve the desired perovskite film morphology: thermal-vacuum deposition,[14] one-step or two-step sequential

Received: January 25, 2021
Accepted: March 24, 2021
Published: April 1, 2021

solution deposition,[15,16] hybrid vapor-assisted solution processes,[17] and so forth. Among these methods, the one-step solution approach is probably the most attractive from an industrial viewpoint due to the easier operation and lower cost. However, one-step precursor solutions usually result in a high density of pinholes and defects. To circumvent this issue, a number of additive engineering strategies have been proposed, proving to be effective in enhancing the film quality and minimizing the recombination losses.[18−21] The incorporation of additives into the photoactive layer is a method widely used also in the fabrication of organic solar cells (OSCs).[22−24] In the context of PSCs, the mechanism behind this strategy is mostly related to the modulation of perovskite crystallization kinetics and to the passivation of defects and trap states. Various types of additives have been successfully applied, including fullerene derivatives,[25] organic solvents, inorganic acids,[26,27] metal halide salts, ionic liquids,[28,29] organic small molecules, and polymers.[30−39] Recently published works have demonstrated that interactions between organic solvents and perovskite components can be conveniently exploited to control the morphology and crystallinity of solution-processed perovskite films.[40−44] Specific features such as a high-boiling point and/or strong Lewis base nature shown by commonly used solvent additives, including 1,8-diiodooctane, *N*-methylpyrrolidone, hexamethylphosphoramide, and dimethyl sulfoxide, have been found to be beneficial to promote the formation of uniform, highly crystalline perovskite films with larger grains.[45−53] However, these solvents generally show high toxicity toward health and environment.

Aiming at the commercialization of PSCs, nontoxicity, ecocompatibility, low-cost, and easy accessibility should be addressed in seeking for the appropriate solvent additives. In this direction, the study herein reported explores for the first time the potential of α-terpineol, a naturally occurring and ecofriendly monoterpene alcohol, as a solvent additive to improve the morphology and crystallinity of one-step solution-processed $CH_3NH_3PbI_{3-x}Cl_x$ (or $MAPbI_{3-x}Cl_x$) perovskite films. Monoterpenes are biogenic chemicals, which currently play an important role in the industrial field as valid and green alternatives to halogenated solvents and chlorofluorocarbons. Among them, in particular, α-terpineol can be isolated from a variety of natural sources such as pine oil, and it is widely employed as a popular fragrance ingredient in perfumes and cosmetics; it also shows promising potential in the biological and medical fields as natural pesticides, antioxidants, anticarcinogenic agents, and so forth.[54] In the context of thin-film solar technologies, α-terpineol is frequently used as a high-viscosity solvent to prepare printable pastes. Its low cost and green nature have already attracted the attention of other research teams working on PSCs, who developed alternative perovskite-deposition approaches involving the use of α-terpineol to disperse the perovskite crystals.[55,56] However, no efficient PSCs based on the use of α-terpineol solvent has been demonstrated yet. Differently from those studies, the present work aims at investigating the potential of α-terpineol in the specific context of additive engineering applications, in order to shed light on the physicochemical perturbations induced by its incorporation into a conventional perovskite solvent system, with the ultimate goal of achieving more efficient and stable PSCs. In this perspective, α-terpineol is also attractive for its high boiling point (bp = 219 °C) compared to that of the major solvent *N*,*N*-dimethylformamide (DMF, bp = 153 °C), and for its hydrophobic nature, both characteristics distinguish it from the other more common alcohols and can favor the formation of more uniform and smooth perovskite films with higher stability under ambient conditions.[55] Moreover, α-terpineol can interact with MA^+ and I^- ions through its −OH group,[56] as well as it can participate in intermediate phases via hydrogen bonding, and this may result in a favorable crystal growth modulation. In this regard, Acik et al. have recently proposed an interesting reaction mechanism for solution-phase perovskite growth in the presence of polar protic alcohol solvents, reflecting the increasing research interest in developing alternative deposition methods based on the use of eco-friendly, nontoxic alcohols.[57]

Thanks to all the aforementioned features, we anticipate that high-quality $MAPbI_{3-x}Cl_x$ perovskite films were successfully deposited from precursor solutions containing green α-terpineol alcohol as a solvent additive; PCEs as high as 17.5% were obtained for planar n−i−p PSCs, along with improved stability and reduced hysteresis. Considering that a very simple, low-cost one-step spin-coating technique was used (without the need of antisolvents), our results are very promising and competitive with those reported in the literature.[33,44,46−53]

2. EXPERIMENTAL SECTION

2.1. Materials. All chemicals were used as received without any further purification. Fluorine-doped tin oxide (FTO)-coated glass slides (TEC7) were purchased from Visiontek Systems. Methylammonium iodide (MAI, 99.9%) was supplied by Ossila. Lead chloride ($PbCl_2$, 99.999%), gold wire (Au, 99.9%), silver wire (Ag, 99.99%), and hydrochloric acid (HCl, 37 wt % aqueous solution) were obtained from Alfa Aesar. Titanium(IV) isopropoxide (99.999%, trace metals basis), molybdenum(VI) oxide (MoO_3, 99.97%, trace metals basis), 4-*tert*-butylpyridine (TBP, 96%), bis(trifluoromethane)-sulfonimide lithium salt (LiTFSI, 99.95%, trace metals basis), chlorobenzene (CB, anhydrous, 99.8%), chloroform (99.0%), acetonitrile (ACN, anhydrous, 99.8%), DMF (anhydrous, 99.8%), isopropyl alcohol (IPA, anhydrous, 99.5%), and α-terpineol (90%) were purchased from Merck Sigma-Aldrich. 2,2′,7,7′-Tetrakis[*N*,*N*-di(4-methoxyphenyl)amino]-9,9-spirobifluorene (spiro-OMeTAD) was supplied by Solaronix.

2.2. Solar Cell Fabrication. FTO-coated glass substrates were cleaned by sonication in acetone and isopropanol, dried under anhydrous N_2 flow, and then kept at 110 °C for approximately 16 h. After this standard cleaning procedure, the substrates were exposed to ultraviolet−ozone treatment for 40 min to remove any organic contamination and improve the wettability of the hydrophobic FTO layer. Immediately after, a compact titania (c-TiO_2) electron-transport layer was deposited by a sol−gel route: a mildly acidic solution of titanium(IV) isopropoxide in isopropanol (titanium isopropoxide/2 M HCl/IPA = 175 μL/17.5 μL/2.5 mL) was spin-coated through a 0.2 μm PTFE filter onto the FTO substrate at 2000 rpm for 60 s, and then calcined in air at 500 °C for 45 min. To prepare the $CH_3NH_3PbI_{3-x}Cl_x$ film, a 3:1 molar ratio of CH_3NH_3I and $PbCl_2$ was dissolved in anhydrous DMF at a concentration of 40 wt %. The obtained precursor solution was dynamically spin-coated onto the TiO_2-coated FTO substrate at 2000 rpm for 20 s, followed by thermal annealing on a hot plate at 105 °C for 1.5 h. To investigate the impact of α-terpineol on the device performance, the additive was incorporated into the $CH_3NH_3PbI_{3-x}Cl_x$ precursor solution at different concentrations, namely, 2.5, 5, 10, 15, and 25 mg mL^{-1}. Subsequently, a hole-transport layer was deposited from a solution consisting of 72.3 mg of spiro-OMeTAD dissolved in 1 mL of CB, 28.8 μL of TBP, and 17.5 μL of a LiTFSI solution (520 mg mL^{-1} in ACN). The solution was spin-coated at 4000 rpm for 45 s. The devices were then stored overnight inside a desiccator under air to allow the oxidation of spiro-OMeTAD. Finally, the top electrode, consisting of 6 nm thick molybdenum suboxide (MoO_x) as the anode

https://doi.org/10.1021/acsaelm.1c00084
ACS Appl. Electron. Mater. 2021, 3, 1813−1825

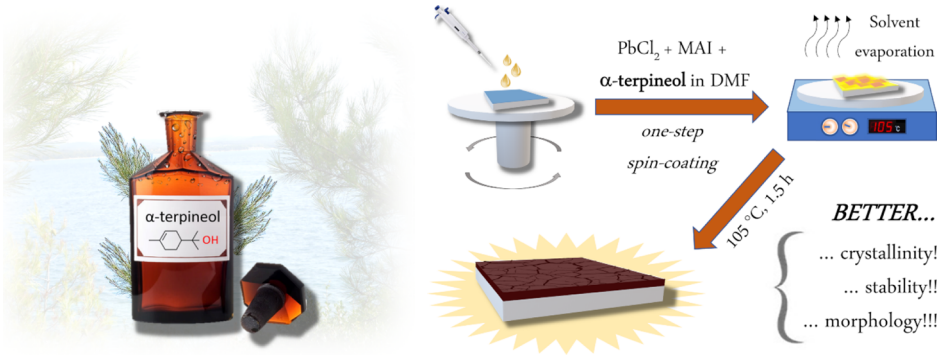

Figure 1. Schematic diagram of the fabrication process proposed in this work, consisting of facile one-step spin-coating of the perovskite precursor solution containing the α-terpineol additive, followed by thermal annealing at 105 °C for 1.5 h, resulting in high-quality $CH_3NH_3PbI_{3-x}Cl_x$ perovskite films.

buffer layer and 100 nm thick Ag or Au as the rear contact, was thermally evaporated through a shadow mask under a vacuum of 5×10^{-6} mbar. The evaporation masks used in this work consist of brass plates with holes drilled in it. The holes were of different diameters, namely 2, 3, 4, and 8 mm, enabling the investigation of the effect of increasing the active area (3.14, 7.07, 12.56, and 50.27 mm^2, respectively) on the device performance. The evaporation rate was set to be 0.3 Å s^{-1} for MoO_x and 2 Å s^{-1} for Ag or Au. Except for the c-TiO_2 deposition, all the processing steps were performed within a glovebox system (Mbraun Inertgas-Systeme GmbH, Germany) filled with N_2 (O_2, H_2O < 0.1 ppm).

2.3. Film and Device Characterization. In-depth characterization of the fabricated thin films and devices was carried out. Fourier transform infrared (FT-IR) spectra were collected in the 4000−600 cm^{-1} range, with a 2 cm^{-1} resolution, using a Bruker-Lumos FT-IR spectrometer (Bruker, Billerica, US-MA) equipped with a Platinum ATR accessory; 60 scans were acquired for each spectrum. X-ray diffraction (XRD) patterns of the perovskite films were collected using a Philips PW 1050/39 diffractometer (Philips Analytical, Almelo, The Netherlands) with Bragg Brentano geometry, equipped with a Ni-filtered Cu Kα radiation source and operated at 40 kV and 30 mA (step 0.1°; counting time 5 s/step). Scanning electron microscopy (SEM) imaging was performed using a FEI Quanta 200 microscope (FEI company, Hillsboro, US-OR) equipped with standard SE and BSE detectors and operated at an accelerating voltage of 30 kV. Energy-dispersive X-ray (EDX) spectra of perovskite films were acquired with an EDAX Genesis XM4i detector (Oxford Instruments, Abingdon-on-Thames, UK). Atomic force microscopy (AFM) imaging was performed by using a Bruker Dimension Icon instrument; all images were acquired in AM tapping mode, using commercially available silicon probes (RTESP type, Bruker) and collecting 512 × 512 points per image. Surface roughness was calculated as the root-mean-square roughness R_q from 2 × 2 μm^2 AFM images. Fluorescence quenching experiments were carried out using a Horiba FluoroMax-4 spectrofluorimeter (HORIBA Jobin Yvon, Edison, US-NJ); the excitation wavelength was fixed at 525 nm, and the spectra were normalized with respect to the absorbance. Absorption spectra of the perovskite films were acquired using an Analytic Jena SPECORD S600 UV−vis spectrophotometer (Analytic Jena AG, Jena, Germany), equipped with a diode array detector and a combination of halogen and deuterium lamps as the light source; the spectra were referenced to a glass slide. Water contact angle measurements were conducted using a DataPhysics Instruments SCA 20 optical contact angle measuring and contour analysis system (DataPhysics Instruments GmbH, Filderstadt, Germany), equipped with a CCD camera with high resolution power, and applying the sessile drop method. The droplet volume was fixed at 10.0 ± 0.5 μL onto the sample surface, while the temperature was set to be 25.0± 0.1 °C for both the support and the injecting syringe. The electrical characterization of the solar cells was accomplished using a Keithley 4200 source-measure unit and a Sunlite Solar Simulator (model 11002, Class ABA; Abet Technologies, Milford, US-CT) equipped with a 100 W xenon arc lamp and an AM 1.5G filter. The simulator was calibrated using a commercial KG5-filtered Si reference cell (model 15151, Abet Technologies) to obtain an incident light power of 100 mW cm^{-2}. All the $J-V$ measurements were performed in a glovebox at room temperature.

3. RESULTS AND DISCUSSION

3.1. Impact of α-Terpineol on Device Performance. In this work, we investigated the effect on the PSC performance of introducing α-terpineol as a solvent additive in the one-step perovskite precursor solution. To this end, PSCs featuring a typical planar n−i−p configuration were fabricated, with compact titania (c-TiO_2) as the electron-transport layer (ETL), $CH_3NH_3PbI_{3-x}Cl_x$ as the photoactive layer, and spiro-OMeTAD as the hole-transport layer (HTL; see the Experimental Section). The energy band diagram of the complete device is sketched in Figure S1 in the Supporting Information. Differently from the traditional mesoscopic PSCs, the absence of a mesoporous metal oxide layer (e.g., mp-TiO_2) in such planar devices leads to an overall simpler but still highly performing architecture, which is better suited for modern PV applications (e.g., flexible solar cells, solar windows, and tandem PV devices). The mixed-halide $CH_3NH_3PbI_{3-x}Cl_x$ perovskite was selected to be the absorber material owing to its well-known and exceptional optoelectronic properties in terms of light absorption and charge transport. In particular, the remarkably high charge-carrier mobilities typical of this perovskite material allow for high PV performances also in the planar device configuration, without the assistance of any mesoporous ETL.[15] The $CH_3NH_3PbI_{3-x}Cl_x$ films were prepared via a one-step solution process, whose simplicity and cost-effectiveness make it attractive also from an industrial viewpoint, and α-terpineol was incorporated in the precursor solution as a solvent additive at different concentrations, as outlined in Figure 1. It is worth noting that the proposed deposition method does not require the use of antisolvents, making the whole process easier and more environmentally friendly (the antisolvent-assisted crystallization typically uses toxic solvents such as CB and toluene).[58]

The perovskite films obtained with the proposed one-step solution approach were then subject to annealing treatment at 105 °C for 1.5 h (step 2 in Figure 1) to promote the conversion of precursors into $CH_3NH_3PbI_{3-x}Cl_x$ crystals. Because α-terpineol has a boiling point (bp = 219 °C) comparable to that of other processing solvents commonly used in PSC fabrication (e.g., γ-butyrolactone, bp = 204 °C), it

https://doi.org/10.1021/acsaelm.1c00084
ACS Appl. Electron. Mater. 2021, 3, 1813−1825

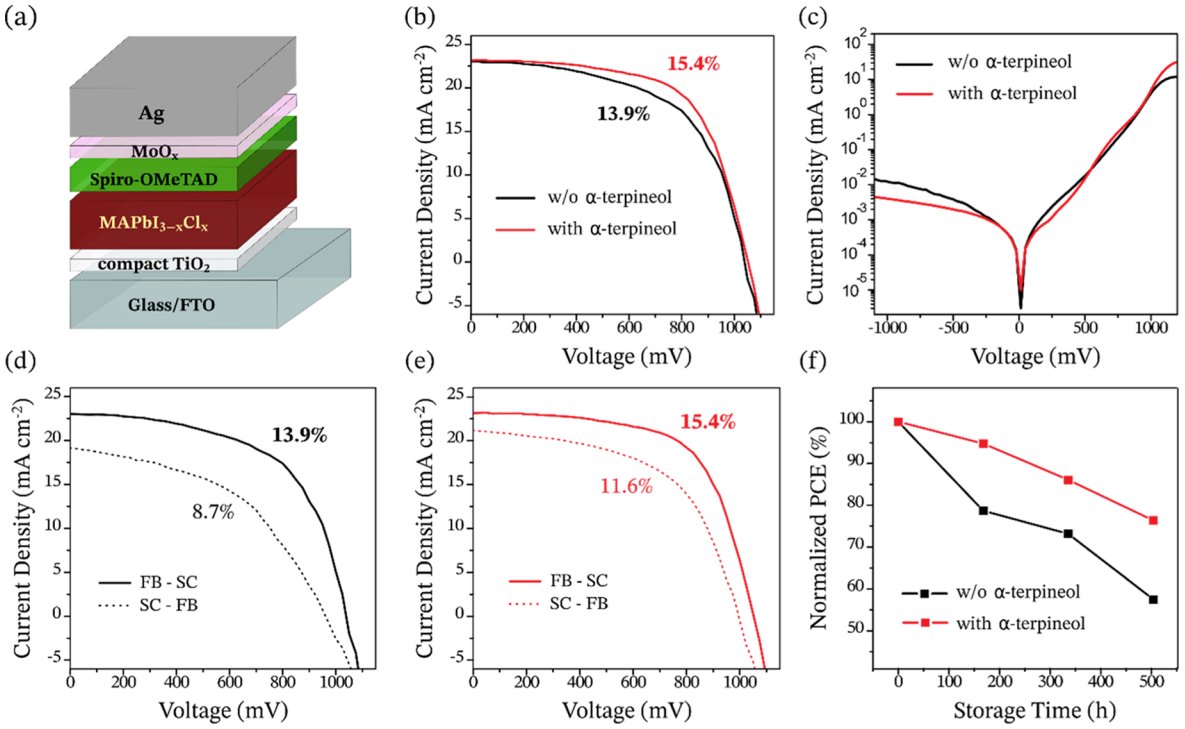

Figure 2. (a) Schematic illustration of the PSC planar n−i−p architecture used in this work. (b) Reverse-scanning $J-V$ curves of the top Ag-based PSCs processed with/without α-terpineol, measured under AM 1.5G illumination. Active area: 3.14 mm^2. (c) Dark $J-V$ curves of the best-performing PSCs processed from solutions with/without α-terpineol. Hysteresis effect in the $J-V$ curves of the top devices prepared using (d) a pristine precursor solution and (e) a precursor solution with 5 mg mL^{-1} α-terpineol by varying the voltage scanning direction, from forward bias to short-circuit and from short-circuit to forward bias. (f) PCE degradation of pristine and α-terpineol-treated cells stored in a glovebox under dark conditions at room temperature.

Table 1. Summary of the Best and Mean Values (from Eight Individual Cells) of PV Parameters Obtained for Ag-Based PSCs Processed from Solutions with/without 5 mg mL^{-1} α-Terpineol, Measured under Standard AM 1.5G Illumination in the Reverse or Forward Voltage Scanning Direction[a]

additive content	scanning direction		J_{sc} [mA cm^{-2}]	V_{oc} [mV]	FF [%]	PCE [%]
0 mg mL^{-1}	reverse	best	23.0	1039	58.2	13.9
	reverse	mean	21.3 (±1.7)	1017 (±32)	57.9 (±5.1)	12.5 (±0.9)
	forward	best	19.1	961	47.0	8.7
5 mg mL^{-1}	reverse	best	23.2	1053	63.1	15.4
	reverse	mean	22.1 (±1.6)	1028 (±26)	62.9 (±3.8)	14.3 (±0.6)
	forward	best	21.2	996	55.1	11.6

[a]The standard deviations around the mean are given in brackets.

is supposed to be completely removed from the samples through evaporation at the end of the annealing step, which ensures high purity of the perovskite film. The hypothesis was lately confirmed by FT-IR spectroscopy measurements (see Figure S2 in the Supporting Information). The FT-IR spectra were collected for substrates where a perovskite film was grown in the presence or the absence of α-terpineol, plus a supplementary substrate where a solution of α-terpineol in chloroform was deposited; the latter sample was prepared in order to retrieve the α-terpineol spectral pattern. After a meticulous analysis, it was possible to observe that the perovskite profile is almost identical for both the two preparation conditions; moreover, the most distinctive features from α-terpineol (the broad O−H stretching band centered at 3368 cm^{-1} and the peak at 1373 cm^{-1} attributed to the O−H bending) were absent in the spectral profile recorded for the perovskite layer grown in the presence of the additive. The collected data suggested that α-terpineol was not retained in the film after thermal annealing. In support of this, no relevant differences in the compositional properties between pristine and α-terpineol-treated $CH_3NH_3PbI_{3-x}Cl_x$ films were observed by EDX analysis (see Figure S3).

After the annealing process, the devices were completed by sequential deposition of the spiro-OMeTAD HTL and the MoO_x/Ag top electrodes to give the final device architecture depicted in Figure 2a. Initially, silver was selected as the metal counter electrode material because of its high conductivity, proper work function (≈4.3 eV), and much lower cost compared to the more commonly used gold, enabling more cost-effective but still highly performing planar n−i−p PSCs to be fabricated. Later on, gold-based devices were also fabricated following the optimized α-terpineol-based procedure in order to maximize the efficiency and investigate the stability under ambient conditions, as will be discussed (see Section 3.4). The as-fabricated devices were then subject to current density−voltage ($J-V$) characterization (see the Experimental Section

https://doi.org/10.1021/acsaelm.1c00084
ACS Appl. Electron. Mater. 2021, 3, 1813−1825

for a detailed description of the setup), and their performance was compared to that of control solar cells processed from pristine precursor solution without additive.

As a first attempt, the effect of three different concentrations of α-terpineol was investigated, namely, 5, 15, and 25 mg mL^{-1}. Surprisingly, the devices processed from the precursor solution containing α-terpineol at a 5 mg mL^{-1} concentration showed a significant PCE enhancement (≈11%) compared to the control solar cells, as presented in Figure 2b. The best performing α-terpineol-treated device possessed a PCE of 15.4% with an open circuit voltage (V_{oc}) of 1053 mV, a short circuit current density (J_{sc}) of 23.2 mA cm^{-2}, and a fill factor (FF) of 63.1%, compared to the 13.9% PCE of the top control device with a V_{oc} of 1039 mV, a J_{sc} of 23.0 mA cm^{-2}, and a FF of 58.2% (see Table 1). On the other hand, the incorporation of α-terpineol at 15 and 25 mg mL^{-1} led to disappointing results. Indeed, a gradual degradation of the PV performance was observed with the increase of the additive concentration (as detailed in Figure S4 and Table S1). This can be ascribed to the poor and nonuniform coverage of the resulting perovskite films, showing an increasing density of striation defects, as evident to the naked eye from the picture in Figure S4. Such radial striated inhomogeneities in the spin-coated films typically arise from unfavorable surface tension effects and are indicative of an inappropriate solvent system. The high viscosity and high boiling point of α-terpineol are very likely to play a critical role in this behavior, making it necessary to use a sufficiently low concentration of the additive in order to prevent excessive and unfavorable changes in the rheological and physical properties of the perovskite ink to be spin-coated. The chemical perturbation of the precursor solution induced by the presence of α-terpineol might also be involved, as will be discussed in the next section.

Based on the above results, two other concentrations of α-terpineol below 15 mg mL^{-1} were attempted, namely 10 and 2.5 mg mL^{-1}. The corresponding $J-V$ curves and PV parameters are reported in Figure S4 and Table S1. The incorporation of 10 mg mL^{-1} α-terpineol caused a significant decrease in the PCE (13.1%) compared to that obtained using 5 mg mL^{-1} α-terpineol (15.4%), and even compared to that of the top control PSC without additive (13.9%), mainly due to a decrease in the J_{sc}. On the other hand, the devices processed from solution containing 2.5 mg mL^{-1} α-terpineol yielded significantly higher PCEs compared to pristine PSCs without additive (14.7% PCE of the best device against 13.9% PCE of the top control PSC). However, the corresponding PV performances were slightly lower than those previously obtained using 5 mg mL^{-1} α-terpineol, thus confirming 5 mg mL^{-1} as the optimum concentration. Although the perovskite films based on 2.5, 5, and 10 mg mL^{-1} additive concentration looked quite similar to the naked eye, SEM imaging revealed a substantially different morphology at the microscale: while the $CH_3NH_3PbI_{3-x}Cl_x$ film deposited from solutions containing 2.5 and 5 mg mL^{-1} α-terpineol appeared very uniform with high surface coverage, the one corresponding to 10 mg mL^{-1} α-terpineol concentration exhibited inhomogeneous morphology with micrometer-sized pinholes (see Figure S4d). Such a limited surface coverage inevitably decreases the probability of photons to be absorbed and converted to a photocurrent, thereby providing a valid explanation to the lower PV performance observed. A more in-depth discussion on the effect of α-terpineol on the perovskite morphology will be provided in the next section.

Focusing on the best results obtained using 5 mg mL^{-1} α-terpineol, the overall increase observed in the PV parameters, and particularly in the FF, compared to the pristine devices indicates that the interface and charge-transport properties can be effectively enhanced by the addition of a proper amount of α-terpineol in the one-step perovskite-deposition process. The decreased series resistance and increased shunt resistance, which can be estimated from the inverse of the slope of the $J-V$ curve at $J = 0$ and at $J = J_{sc}$ (see Figure 2b), reveal faster charge transport and reduced carrier recombination and suggest an enhanced quality of the perovskite film in terms of coverage, uniformity, and crystallinity, as will be confirmed. The dark $J-V$ curves of the PSCs with and without α-terpineol are also reported in Figure 2c. It is observed that the dark current density of the device with α-terpineol is lower than that of the control cell in the reverse bias region, indicating that the leakage current is reduced with the addition of α-terpineol. On the other hand, the dark current density is higher for the α-terpineol-based device under the forward bias (voltages higher than 1 V), suggesting a lower injection barrier at the TiO_2/perovskite interface. These results account for the increase in V_{oc} and FF observed under standard illumination.

Figure 2d,e compares the hysteretic behavior of the control PSCs and the PSCs prepared with 5 mg mL^{-1} α-terpineol solution depending on the voltage scanning direction. The control device showed a relatively large degree of hysteresis, with the lowest PCE (8.7%) corresponding to the forward scan. Such hysteresis effects may arise from charge trapping/detrapping dynamics resulting from a large defect density in the perovskite film, as well as from injection barriers at the perovskite/charge-transport layer interfaces.[10] Interestingly, the cell using α-terpineol in the precursor yielded a PCE of 11.6% under forward voltage scanning, revealing a significantly reduced hysteresis and a much-improved FF. These results further suggest a reduced nonradiative recombination in the α-terpineol-modified perovskite film and lower carrier injection barriers at the interfaces, which translate into higher performances and lower hysteresis.

The reproducibility of the PV performances was also analyzed. The values shown in Table 1 are average values and standard deviations of eight devices fabricated under identical conditions, with or without α-terpineol. The average V_{oc}, J_{sc}, FF, and PCE for the eight control cells are (1017 ± 32) mV, (21.3 ± 1.7) mA cm^{-2}, (57.9 ± 5.1)%, and (12.5 ± 0.9)%, respectively, measured under reverse voltage scanning. On the other hand, the average V_{oc}, J_{sc}, FF, and PCE for the eight devices prepared from α-terpineol-based solutions are (1028 ± 26) mV, (22.1 ± 1.6) mA cm^{-2}, (62.9 ± 3.8)%, and (14.3 ± 0.6)%, respectively, extracted from the reverse-scanning $J-V$ curves. It is clear from the lower standard deviations that adding α-terpineol in the precursor solution significantly improves the reproducibility of PSCs. This means that the proposed deposition method can generate compact and highly repeatable perovskite films. Considering that a very simple one-step spin-coating technique was used in this work (without the need of antisolvent treatment), the achieved PCEs, along with the high reproducibility of the fabricated PSCs, are surprisingly good and very competitive with those of other PV systems with analogous characteristics reported in the literature, as well as comparable with those of other PV devices featuring more sophisticated structures/compositions and/or based on the use of toxic additives (as detailed in Table S2 in the Supporting Information).

https://doi.org/10.1021/acsaelm.1c00084
ACS Appl. Electron. Mater. 2021, 3, 1813−1825

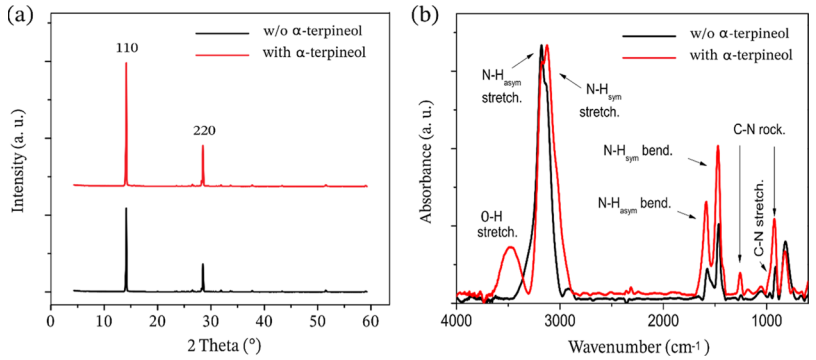

Figure 3. (a) XRD patterns of the perovskite films processed from one-step precursor solutions without/with α-terpineol, showing the characteristic peaks of the $CH_3NH_3PbI_{3-x}Cl_x$ tetragonal phase with predominant crystallization along the (110) and (220) lattice planes. (b) Normalized FT-IR spectra of pre-annealed perovskite precursor films deposited by spin-coating the perovskite precursor solutions without/with α-terpineol on top of c-TiO_2/FTO-coated glass substrates, as obtained before thermal annealing.

The inherent stability of the Ag-based PSC devices with and without the α-terpineol additive was also investigated. The solar cells were stored in a N_2-filled glovebox in the dark, and their PV performance was measured at different time intervals at room temperature. The results reported in Figure 2f and Table S3 in the Supporting Information show that, after more than 500 h of storage, the PCE of the best α-terpineol-based device degraded only to around 76% of its initial value. On the other hand, the top control device merely retained 58% of its original efficiency, mainly due to a fast decrease in the J_{sc}. Because the control and modified devices were processed and stored under identical conditions, this discrepancy can be entirely attributed to the effect of α-terpineol on the intrinsic properties of the perovskite layer. It is known from the literature that the perovskite materials can undergo several decomposition mechanisms, and that the latter are favored by a high density of defects and grain boundaries in the perovskite film.[11] Therefore, the enhanced stability observed in the α-terpineol-based devices suggests that the incorporation of this additive in the precursor solution can effectively prevent or retard the degradation of the perovskite by favorably altering the crystallization kinetics and the final morphology of the spin-coated film.

As widely discussed in the literature, another major challenge in PSC manufacturing is the scaling up.[2] In large-area PSC devices, surfaces, bulk defects, and interfaces introduce charge recombination centers that lead to non-radiative losses and a consequent decrease in the PV parameters. The dilemma with fabricating large-area devices is that the perovskite layer should be thin enough to minimize resistive losses, while at the same time, it should cover the entire area in a contiguous and uniform manner. However, the deposition of uniform and pinhole-free perovskite films over a large area using a simple solution-based technique such as spin-coating is typically arduous, especially in the case of one-step solution approaches. In this work, solar cells with an increasing active area (3.14, 7.07, 12.56, and 50.27 mm^2) were fabricated in order to evaluate the impact of the α-terpineol additive on the device performance while scaling up. The active-area-dependent $J-V$ curves of the top devices with and without additives are shown in Figure S5, together with the trends of the corresponding conversion efficiencies. The PV parameters are summarized in Table S4. A significant decrease in the conversion efficiency with the increase of the active area was observed for the control devices. The decrease in the FF (from 58.2 to 42.1%) was the most significant influence, as often reported in the literature. Indeed, the FF parameter is strictly linked to charge transport and recombination, which in turn depend on the morphology of the perovskite film over the entire active area. Opposite to the control devices, the solar cells processed using α-terpineol as a solvent additive showed a minor reduction of the PV parameters as the active area increased. The FF decreased only from 63.1 to 59.4% when the active area was increased by 16 times from 3.14 to 50.27 mm^2. A PCE as high as 14.0% was achieved for the α-terpineol-based PSC with a 12.56 mm^2 active area, while an acceptable PCE of 10.4% (against 6.0% of pristine device) was retained after further increasing the active area up to 50.27 mm^2. This implies that the incorporation of α-terpineol into the one-step precursor solution improves the quality of the perovskite film over a larger area.

3.2. Structural and Morphological Analyses. From the results shown so far, the incorporation of α-terpineol into the perovskite precursor solution generates a significant enhancement in the PV performance of the devices. To explore the mechanism behind this improvement, the structural and morphological properties of the perovskite films with and without the α-terpineol additive were opportunely analyzed and compared. First, XRD measurements were conducted to investigate the role of α-terpineol in perovskite crystallization. The analysis results are reported in Figure 3a. Both control and modified films exhibited prominent peaks at 14.1 and 28.5°, which can be ascribed to the (110) and (220) lattice planes of the typical $CH_3NH_3PbI_{3-x}Cl_x$ tetragonal phase, respectively. The unchanged positions of the peaks suggest that the solvent additive does not modify the crystal structure of the perovskite. On the other hand, the evident variations in intensity are indicative of a higher degree of crystallinity. Specifically, the increased intensity of the two main peaks in comparison with the others, such as the peak at 31.9° attributable to the (310) lattice plane, observed after adding α-terpineol in the precursor solution indicates that the α-terpineol-treated samples exhibit crystallites with a more pronounced orientation. Highly oriented crystalline structures are typically advantageous to charge carrier transport within the perovskite layer.[59] Such an enhanced crystallinity of the perovskite film generally leads to higher PCEs, reduced hysteresis, and improved stability of PSCs, and this is in perfect agreement with the results of the $J-V$ analysis shown so far.

https://doi.org/10.1021/acsaelm.1c00084
ACS Appl. Electron. Mater. 2021, 3, 1813−1825

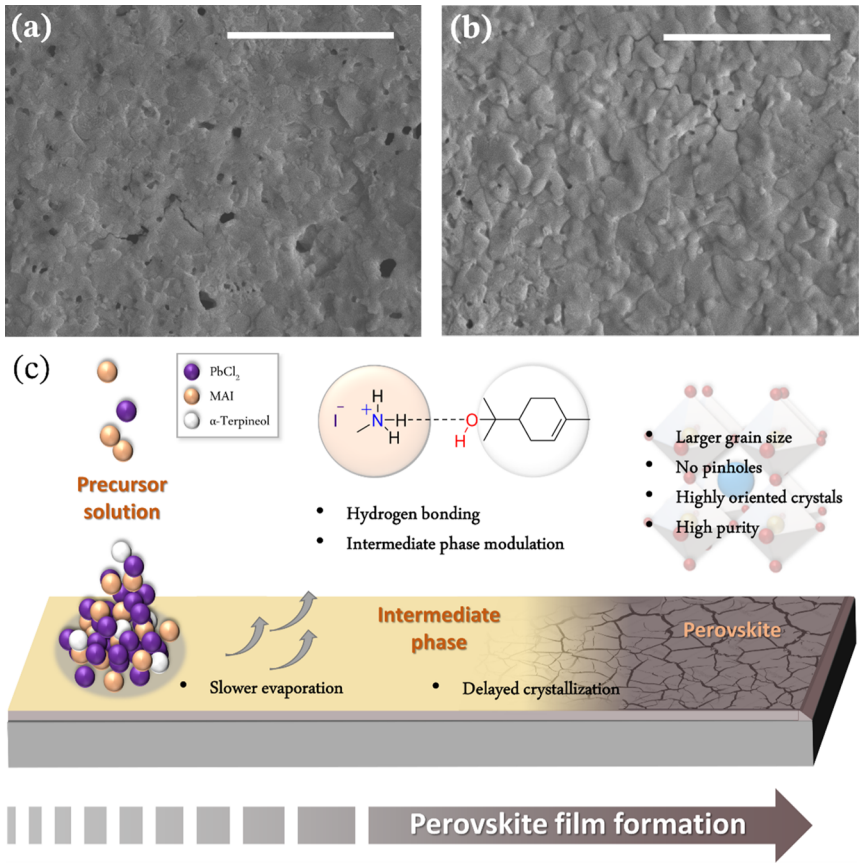

Figure 4. Top-view SEM images of $CH_3NH_3PbI_{3-x}Cl_x$ perovskite films spin-coated on top of c-TiO_2/FTO-coated glass substrates from (a) a pristine precursor solution without the additive and (b) a precursor solution with 5 mg mL^{-1} α-terpineol concentration. Scale bar: 5 μm. (c) Illustration of the roles of the α-terpineol additive in the perovskite film formation.

Because α-terpineol can be retained in the film for a longer time compared to DMF due to its higher boiling point, it is supposed that the residual α-terpineol can helpfully balance the dissolution and recrystallization processes during the annealing treatment, retarding the nucleation time and promoting the formation of higher quality perovskite crystals. The chemical interactions between the −OH group in α-terpineol and the MA^+ and I^- ions in the perovskite precursor may also be responsible for the improved crystallization. Indeed, it is well known that the forces induced by additives between anions and cations of the perovskite precursor, such as hydrogen bonds, play a critical role in the formation of highly crystalline perovskite films.[18] Evidence of these kinds of interactions between α-terpineol and perovskite has already been reported in the literature.[56] To provide further evidence, the FT-IR spectra were collected for pristine and α-terpineol-based perovskite precursor films obtained immediately after spin-coating the corresponding precursor solutions without and with α-terpineol onto c-TiO_2/FTO-coated glass substrates and by not subjecting them to any thermal treatment (pre-annealed precursor films); this is done in order to shed light on the chemical perturbation induced by α-terpineol while it is still present in the film before evaporation. The corresponding spectra are reported in Figure 3b. The spectra show similar profiles, with the major bands attributable to the N−H bond stretching related to the MA^+ residue (3200−3000 cm^{-1}), while the features located between 1700 and 1400 cm^{-1} can be ascribed to both symmetric and asymmetric bending modes involving N−H bonds; moving to the fingerprint region, other bands can be identified, such as C−N stretching and rocking modes.[60] A more in-depth analysis of those peaks provided some useful insights. First, all the bands associated with N−H bending and C−N stretching/rocking modes resulted to be shifted to higher wavenumbers (10−20 cm^{-1}) in the case of the α-terpineol-based sample. Because the two samples without/with an additive were prepared and handled under the same conditions, the observed shifts clearly indicate that the α-terpineol has an interaction with the perovskite precursor. More specifically, this change can be explained by the formation of hydrogen bonds between the organic cation MA^+ in the perovskite precursor and the −OH functional group in α-terpineol, which could lead to the formation of an organic cation—α-terpineol precursor complex. This in turn would reduce/delay the incorporation of MAI into the perovskite structure, with evident changes in the IR signatures.[61] In this regard, Figure S6 directly compares the FT-IR spectra of MAI and $MAPbI_{3-x}Cl_x$, providing valuable insights into the impact of the different chemical environments experienced by MAI inside and outside the 3D perovskite cage. Similar mechanisms of selective complexation of the organic cation induced by additives containing −OH groups has already been reported in the literature, resulting in a delayed crystallization process and consequently improved crystallinity and grain size of the perovskite film.[39]

Proceeding with the FT-IR analysis, it is worth mentioning the evolution of the spectral features related to the N−H bond stretching modes (see Figure 3b): in fact, in addition to a slight red shift, it was possible to reveal a variation in the relative

https://doi.org/10.1021/acsaelm.1c00084
ACS Appl. Electron. Mater. 2021, 3, 1813−1825

intensities corresponding to the asymmetric and symmetric stretching modes, which favors the symmetric stretching mode in the case of the sample prepared using α-terpineol as a solvent additive. A similar trend can be observed in the case of MAI compared to $MAPbI_{3-x}Cl_x$ (see Figure S6), in support of the hypothesis of a reduced/delayed MAI inclusion in the perovskite structure due to the presence of the α-terpineol molecules. Such evidence is corroborated by the literature, where it is widely reported how N−H stretch vibrations are sensitive to the modification of the interaction strength between MA^+ and I^- ions induced by molecular systems with hydrogen bonding capability.[60,62] Therefore, it can be inferred that the −OH groups in the α-terpineol molecules are capable of perturbating the chemical environment in such a way that they affect the interaction between the methylammonium and the iodide, thus modulating the process and kinetics of intermediate phase formation and resulting in the improvement of the quality of the perovskite film.

After clarifying the effects of α-terpineol on the perovskite precursor, we analyzed the morphology of the resulting perovskite films processed in the presence or absence of α-terpineol by SEM and AFM. The corresponding images are shown in Figures 4 and S7, respectively. As evident from the top-view SEM images, the pristine perovskite film exhibited relatively small grains with apparent pinholes and grain boundaries (Figure 4a), as typically expected from one-step solution-deposition processes. As previously mentioned, these defects can introduce nonradiative recombination centers and shunting paths, causing energy loss, and thus reducing the overall PV performance. The addition of α-terpineol led to a significant improvement in the morphology of the one-step solution-processed $CH_3NH_3PbI_{3-x}Cl_x$ films, which appeared more uniform and homogenous with larger grain sizes and no pinholes (Figure 4b). This result suggests that the additive is capable of modulating the perovskite crystallization process and kinetics in such a way as to obtain a dense and pinhole-free surface, promoting the growth of larger $CH_3NH_3PbI_{3-x}Cl_x$ grains, and reducing the voids between perovskite domains.

According to the AFM results (see Figure S7 in the Supporting Information), the control films appeared relatively rough (R_q = 53.6 nm) and unshaped, as frequently reported in the literature for one-step spin-coated perovskite layers. On the other hand, the films prepared from α-terpineol-based solution displayed a better surface coverage, lower roughness (R_q = 43.5 nm), and more regular shaped crystallites. This is consistent with a slower and controlled crystallization of the perovskite induced by the residual α-terpineol during the thermal treatment, which helps to get a more uniform deposition and a smoother morphology.

Based on the above results, we propose a schematic diagram illustrating the mechanism of action of the α-terpineol additive as shown in Figure 4c. The α-terpineol additive plays a multifunctional role in the perovskite film formation, by reducing the solvent evaporation rate during the spin-coating process (due to its higher boiling point) and, at the same time, chemically interacting with the perovskite precursors through hydrogen bonding (by means of its −OH group). In doing so, it favors a slower and controlled release of (and reaction between) the perovskite precursors, modulating the intermediate phase formation and assisting the growth of pinhole-free, large grain-sized, and highly crystalline perovskite films. The additive is then completely removed from the perovskite film together with the processing solvent after the thermal annealing treatment, facilitating higher purity of the resulting perovskite crystals. The observed improvements in the morphological and structural properties of the perovskite films induced by α-terpineol are typically advantageous to charge transport/extraction in the corresponding PSCs, and thus provide a valid explanation for the higher PCEs observed for the α-terpineol-treated solar cells.

3.3. Optical Characterization of Perovskite Films. To further understand how the α-terpineol additive influences the performances of PSCs, steady-state photoluminescence (PL) measurements were performed for both the control samples and the α-terpineol-treated samples. Indeed, steady-state PL spectra can provide useful information about the quality of thin films and interfaces in PSCs; by monitoring the variations in fluorescence intensity, it is possible to evaluate the magnitude of nonradiative recombination losses in pristine perovskite films as well as the efficiency of charge transfer processes at the interfaces. The steady-state PL data were recorded once fixing the excitation wavelength at 525 nm to incident from the FTO/glass side, and the resulting spectra are shown in Figure 5.

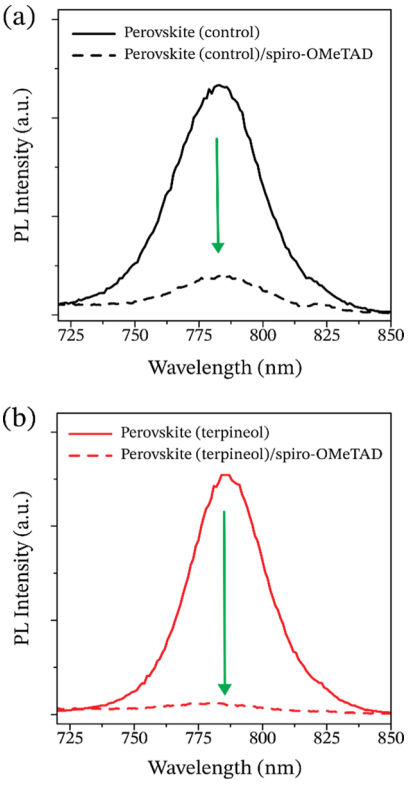

Figure 5. Steady-state PL spectra of the control (a) and α-terpineol-treated (b) perovskite films with/without (solid line/dashed line) spiro-OMeTAD HTL spin-coating on top of them, showing the characteristic fluorescence of $CH_3NH_3PbI_{3-x}Cl_x$ and the fluorescence quenching (green arrow) caused by the deposition of spiro-OMeTAD.

Both control and α-terpineol-treated perovskite films exhibited a prominent emission band centered at ≈783 nm, corresponding to the characteristic fluorescence of $CH_3NH_3PbI_{3-x}Cl_x$. Figure 5 underlines that there is a clear fluorescence quenching caused by deposition of spiro-OMeTAD on top of the perovskite films. This quenching is more pronounced in the case of α-terpineol-treated sample

https://doi.org/10.1021/acsaelm.1c00084
ACS Appl. Electron. Mater. 2021, 3, 1813−1825

(92%) compared to the control sample (79%). This is indicative of a better interface contact and a more efficient charge transfer process (which competes with radiative recombination) at the perovskite/spiro-OMeTAD junction. Therefore, the enhanced quality of the α-terpineol-treated perovskite film seems to positively impact the interface and charge transport properties of the device, as expected. This further justifies the improved PV performance and enhanced stability previously observed.

Figure S8 directly compares the optical (absorption + fluorescence) properties of control and α-terpineol-treated perovskite films. No relevant differences in the absorption spectra were revealed (Figure S8a). Both samples exhibited an absorption band edge at about 780 nm, which is consistent with the optical bandgap of $CH_3NH_3PbI_{3-x}Cl_x$ (≈1.6 eV), and comparable absorption intensities in the measured wavelength range. This implies that the discrepancy of the J_{sc} and V_{oc} values between control devices and α-terpineol-processed devices is not due to an enhanced light absorption or to a variation of the bandgap, but it is more related to charge recombination mechanisms. On the other hand, the addition of α-terpineol apparently improves the fluorescence efficiency of the pristine $CH_3NH_3PbI_{3-x}Cl_x$ film, as evident from the increased PL peak intensity in Figure S8b. This may indicate a reduced density of defects (where emission might be quenched) and trapping sites for nonradiative recombination within the perovskite film, which would be consistent with the improved quality of the perovskite grains revealed by XRD and SEM and with the enhanced performance and stability exhibited by the α-terpineol-treated devices. A slight red shift of PL peak was also observed after introduction of the α-terpineol additive, which might be caused by a minor adjustment of the energy level position or by the variation in the perovskite grain size.

In summary, the results of the steady-state PL analysis further demonstrate the beneficial impact of the α-terpineol additive on the interface and charge transport properties of the perovskite film as a direct consequence of the improved morphology/crystallinity.

3.4. Performance and Stability of Au-Based Devices.

The overall beneficial impact of the α-terpineol additive on the perovskite film quality could provide the devices with long-term stability also under ambient humidity conditions. To investigate this possibility, α-terpineol-treated devices with gold top electrodes were also fabricated (see Figure 6a), in order to prevent stability issues related to the use of silver in PSCs and under an ambient atmosphere.[63] Indeed, the well-known instability of the Ag/perovskite interface under ambient conditions (without encapsulation) causes a severe drop in PCE for both pristine and α-terpineol-modified devices (as evident from Figure S9), hindering a more focused analysis of the effect of α-terpineol on the air stability of the perovskite film for a longer term. Therefore, even though Ag-based architectures certainly constitute a more cost-effective solution and can be stabilized against external stimuli through various strategies (e.g., encapsulation, diffusion barriers, and so forth), we found it interesting to study the behavior of Au-based α-terpineol-treated PSCs in order to obtain information about their intrinsic environmental stability. Their performances were opportunely compared with those of control solar cells prepared without using α-terpineol and featuring gold top electrodes as well. The results of the $J-V$ analysis are summarized in Table 2.

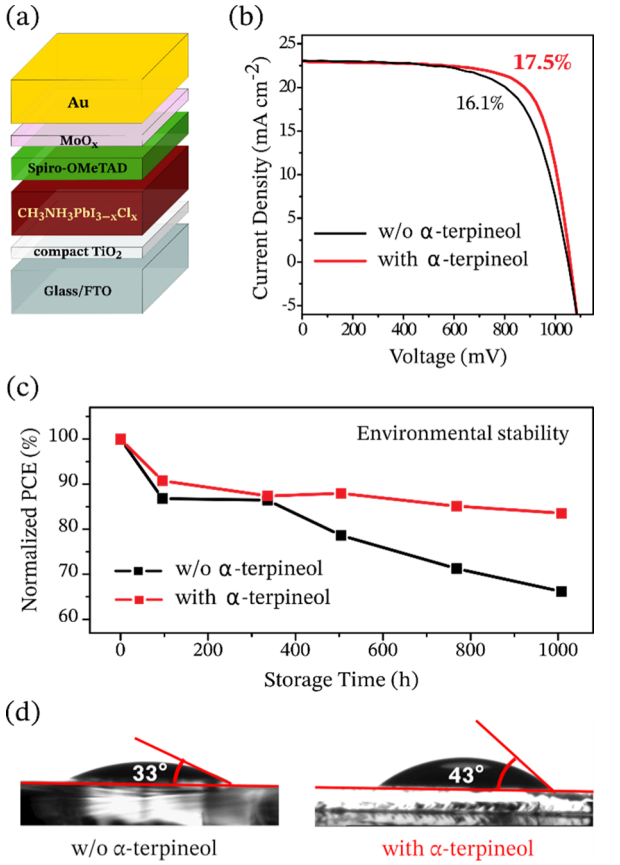

Figure 6. (a) Device structure of PSCs fabricated using Au top electrodes. (b) Reverse-scanning $J-V$ curves of the top Au-based PSCs prepared from solutions with/without α-terpineol. (c) PCE decays of the top control and α-terpineol-treated Au-based devices exposed to ambient air under dark conditions without encapsulation. (d) Water contact angle of perovskite films processed from solutions without and with α-terpineol.

Table 2. PV Parameters of the Best-Performing Au-Based PSCs Processed with/without α-Terpineol under Reverse/Forward Voltage Scanning Obtained under Standard 1 sun Illumination

additive content	J_{sc} [mA cm^{-2}]	V_{oc} [mV]	FF [%]	PCE [%]
0 mg mL^{-1} (reverse)	23.1	1051	66.2	**16.1**
0 mg mL^{-1} (forward)	22.7	1031	55.1	12.9
5 mg mL^{-1} (reverse)	23.0	1059	72.1	**17.5**
5 mg mL^{-1} (forward)	22.9	1033	65.9	15.6

Despite the cost, it is well known from the literature that gold generally leads to the best-performance devices owing to its high work function (5.1 eV) and excellent chemical stability.[64] In this work, a record high PCE of 17.5% was achieved under reverse scan (see Figure 6b), confirming the superiority of gold as a counter electrode material as well as the effectiveness of α-terpineol as a solvent additive (see Table 2). The higher FF and V_{oc} values obtained for the Au-based devices are indicative of an improved interface contact and reduced charge carrier recombination compared with the Ag-based cells, as expected. As evident from Figure 6b, the beneficial impact of α-terpineol on the PV performance was confirmed also for the Au-based devices, with a substantial PCE increase (from 16.1 to 17.5%). Moreover, similar improvements to that shown by the Ag-based PSCs (see

https://doi.org/10.1021/acsaelm.1c00084
ACS Appl. Electron. Mater. 2021, 3, 1813−1825

Figure 2) were observed for the Au-based devices after incorporation of α-terpineol in terms of current rectifying ability and hysteretic behavior, as reported in Figure S10 in the Supporting Information.

Time-dependent $J-V$ measurements were carried out to evaluate the PCE degradation of the Au-based, α-terpineol-treated solar cells when exposed to ambient air under dark conditions without encapsulation. While the control devices experienced relatively rapid PCE degradation after aging, mainly attributable to perovskite decomposition, the use of α-terpineol helped restrains the sensitivity of the perovskite films to humidity and maintain the stability of the devices. As reported in Figure 6c, the PCE of the top control cell degraded to 65% of its initial value after 1000 h of storage, whereas the best device treated with α-terpineol maintained 84% of its initial PCE, yielding an efficiency as high as 14.7% (with J_{sc} = 21.6 mA cm^{-2}, V_{oc} = 1019 mV, and FF = 66.5%) after the same time frame.

To further investigate the resistance of the $CH_3NH_3PbI_{3-x}Cl_x$ films against moisture, water contact angle measurements were carried out. Figure 6d presents the contact angle of water droplets on top of the control and modified perovskite films, with the corresponding values of 33 and 43°, respectively. It can be seen that the hydrophobicity of the perovskite film increases after introduction of α-terpineol. Such a behavior has already been reported in the literature for high-quality perovskite films obtained via Ostwald ripening.[65] An increased hydrophobicity implies enhanced humidity tolerance under air, with consequently retarded perovskite decomposition, confirming that the proposed additive-assisted deposition method can be effectively used to stabilize the perovskite crystals and prevent moisture degradation.

The above results demonstrate that the impact of α-terpineol on the perovskite film formation can also help in enhancing the perovskite resistance against moisture and prolonging the device lifetime in an ambient environment, as highly coveted. These remarkable achievements constitute a spur to explore the potential of other green, eco-sustainable substances with properties similar to those of α-terpineol (high boiling point, polar protic nature, etc.) as solvent additives, including other monoterpenoids. Moreover, the proposed one-step deposition approach can be used in the preparation of PSCs with more complex and more performing perovskite compositions (e.g., triple cation mixed-halide perovskites) and/or device architectures (e.g., mesoscopic PSCs), thanks to its versatility and reproducibility, in the ultimate goal of achieving record PCEs, prolonged lifespan, and totally suppressed hysteresis.

4. CONCLUSIONS

In this work, nontoxic, eco-compatible α-terpineol was successfully employed as a solvent additive in the fabrication of high-performance planar n−i−p PSCs. It was demonstrated that the incorporation of a proper amount of α-terpineol into the one-step perovskite precursor solution can lead to perovskite films with improved crystallinity, lower roughness, reduced concentration of defects and grain boundaries, and high purity with negligible additive residues. The higher boiling point of α-terpineol compared to the major solvent (DMF), along with its capability of interacting with the perovskite precursors through its hydroxyl group, beneficially impacts the crystallization process and kinetics of $CH_3NH_3PbI_{3-x}Cl_x$, favoring the formation of a continuous and homogenous film with a smoother morphology and a larger grain size. Planar n−i−p PSCs processed from solutions containing α-terpineol and featuring Ag top electrodes exhibited a maximum PCE of 15.4%, which is significantly higher than that yielded by control devices without additives (13.9%). The PV parameters (V_{oc}, J_{sc}, and FF) and inherent stability of the devices were all improved due to reduced nonradiative recombination, and the hysteresis effect was partially eliminated. By replacing Ag with Au as the metal top electrode, the PCE was further enhanced up to 17.5%, which is remarkable considering that the devices were prepared using a simple planar architecture and basic perovskite composition.

The proposed additive-assisted one-step deposition method may have universal applicability for different perovskite compositions, it is highly reproducible, and it can be readily scaled up to larger device areas without the need of antisolvents, which are typically toxic and environmentally unfriendly. Moreover, it was demonstrated that it can provide the perovskite films with enhanced water resistance and stability under ambient humidity conditions. These results constitute a step forward on the long road to a complete removal of toxic solvents from PSC fabrication protocols, as well as they are encouraging with respect to the scaling up and a long-term lifespan of PSCs in the prospect of a future commercialization.

■ ASSOCIATED CONTENT

Supporting Information

The Supporting Information is available free of charge at https://pubs.acs.org/doi/10.1021/acsaelm.1c00084.

Energy band diagram of the fabricated devices; FT-IR spectra, EDX spectra, and SEM and AFM images of the perovskite films; $J-V$ characterization as functions of the α-terpineol concentration and the active area; and dark $J-V$ curves and $J-V$ hysteresis of the Au-based devices (PDF)

■ AUTHOR INFORMATION

Corresponding Author

Bruno Pignataro − *Department of Physics and Chemistry—Emilio Segrè, University of Palermo, 90128 Palermo, Italy; INSTM—Palermo Research Unit, 90128 Palermo, Italy;* orcid.org/0000-0003-3003-9144; Email: bruno.pignataro@unipa.it

Authors

Giuliana Giuliano − *Department of Physics and Chemistry—Emilio Segrè, University of Palermo, 90128 Palermo, Italy;* orcid.org/0000-0001-9240-3699

Aurelio Bonasera − *Department of Physics and Chemistry—Emilio Segrè, University of Palermo, 90128 Palermo, Italy; INSTM—Palermo Research Unit, 90128 Palermo, Italy;* orcid.org/0000-0003-3275-6809

Michelangelo Scopelliti − *Department of Physics and Chemistry—Emilio Segrè, University of Palermo, 90128 Palermo, Italy; INSTM—Palermo Research Unit, 90128 Palermo, Italy; Consorzio Interuniversitario di Ricerca in Chimica dei Metalli nei Sistemi Biologici (C.I.R.C.M.S.B.), 70121 Bari, Italy;* orcid.org/0000-0001-5931-7668

Delia Chillura Martino − *INSTM—Palermo Research Unit, 90128 Palermo, Italy; Department of Biological, Chemical, and Pharmaceutical Sciences and Technologies (STeBiCeF),*

University of Palermo, 90128 Palermo, Italy; orcid.org/0000-0001-5141-7285

Tiziana Fiore − *Department of Physics and Chemistry—Emilio Segrè, University of Palermo, 90128 Palermo, Italy; Consorzio Interuniversitario di Ricerca in Chimica dei Metalli nei Sistemi Biologici (C.I.R.C.M.S.B.), 70121 Bari, Italy*

Complete contact information is available at: https://pubs.acs.org/10.1021/acsaelm.1c00084

Author Contributions

This manuscript was written through contributions of all authors. All authors have given approval to the final version of the manuscript.

Notes

The authors declare no competing financial interest.

■ ACKNOWLEDGMENTS

Italian MiUR (Ministero dell'Istruzione, dell'Università e della Ricerca) is acknowledged for funding through the program PON 12 aree di specializzazione PNR 2015-2020 (project "BEST4U—Tecnologia per celle solari bifacciali ad alta efficienza a 4 terminali per utility scale", CUP B61B19000160005). MiUR is also acknowledged for funding through the program PON "AIM: Attrazione e Mobilità Internazionale", call AIM1809078-2 and CUP B78D19000280001. The Advanced Technologies Network (ATeN) Center (University of Palermo; project "Mediterranean Center for Human Health Advanced Biotechnologies (CHAB)", PON R&C 2007-2013) is also acknowledged for hospitality and service.

■ REFERENCES

(1) Jena, A. K.; Kulkarni, A.; Miyasaka, T. Halide Perovskite Photovoltaics: Background, Status, and Future Prospects. *Chem. Rev.* **2019**, *119*, 3036−3103.

(2) Roy, P.; Kumar Sinha, N.; Tiwari, S.; Khare, A. A Review on Perovskite Solar Cells: Evolution of Architecture, Fabrication Techniques, Commercialization Issues and Status. *Sol. Energy* **2020**, *198*, 665−688.

(3) Mora-Seró, I.; Saliba, M.; Zhou, Y. Towards the Next Decade for Perovskite Solar Cells. *Sol. RRL* **2020**, *4*, 1900563.

(4) NREL. Best Research-Cell Efficiency Chart. https://www.nrel.gov/pv/cell-efficiency.html (accessed Jan 13, 2021).

(5) Yang, D.; Yang, R.; Priya, S.; Liu, S.; Frank. Recent Advances in Flexible Perovskite Solar Cells: Fabrication and Applications. *Angew. Chem., Int. Ed.* **2019**, *58*, 4466−4483.

(6) Shi, B.; Duan, L.; Zhao, Y.; Luo, J.; Zhang, X. Semitransparent Perovskite Solar Cells: From Materials and Devices to Applications. *Adv. Mater.* **2020**, *32*, 1806474.

(7) Giuliano, G.; Cataldo, S.; Scopelliti, M.; Principato, F.; Chillura Martino, D.; Fiore, T.; Pignataro, B. Nonprecious Copper-Based Transparent Top Electrode via Seed Layer−Assisted Thermal Evaporation for High-Performance Semitransparent n-i-p Perovskite Solar Cells. *Adv. Mater. Technol.* **2019**, *4*, 1800688.

(8) Liu, C.; Cheng, Y.-B.; Ge, Z. Understanding of Perovskite Crystal Growth and Film Formation in Scalable Deposition Processes. *Chem. Soc. Rev.* **2020**, *49*, 1653−1687.

(9) Luo, D.; Su, R.; Zhang, W.; Gong, Q.; Zhu, R. Minimizing Non-Radiative Recombination Losses in Perovskite Solar Cells. *Nat. Rev. Mater.* **2020**, *5*, 44−60.

(10) Liu, P.; Wang, W.; Liu, S.; Yang, H.; Shao, Z. Fundamental Understanding of Photocurrent Hysteresis in Perovskite Solar Cells. *Adv. Energy Mater.* **2019**, *9*, 1803017.

(11) Boyd, C. C.; Cheacharoen, R.; Leijtens, T.; McGehee, M. D. Understanding Degradation Mechanisms and Improving Stability of Perovskite Photovoltaics. *Chem. Rev.* **2019**, *119*, 3418−3451.

(12) Gao, F.; Zhao, Y.; Zhang, X.; You, J. Recent Progresses on Defect Passivation toward Efficient Perovskite Solar Cells. *Adv. Energy Mater.* **2020**, *10*, 1902650.

(13) Tailor, N. K.; Abdi-Jalebi, M.; Gupta, V.; Hu, H.; Dar, M. I.; Li, G.; Satapathi, S. Recent Progress in Morphology Optimization in Perovskite Solar Cell. *J. Mater. Chem. A* **2020**, *8*, 21356−21386.

(14) Liu, M.; Johnston, M. B.; Snaith, H. J. Efficient Planar Heterojunction Perovskite Solar Cells by Vapour Deposition. *Nature* **2013**, *501*, 395−398.

(15) Stranks, S. D.; Eperon, G. E.; Grancini, G.; Menelaou, C.; Alcocer, M. J. P.; Leijtens, T.; Herz, L. M.; Petrozza, A.; Snaith, H. J. Electron-Hole Diffusion Lengths Exceeding 1 Micrometer in an Organometal Trihalide Perovskite Absorber. *Science* **2013**, *342*, 341−344.

(16) Burschka, J.; Pellet, N.; Moon, S.-J.; Humphry-Baker, R.; Gao, P.; Nazeeruddin, M. K.; Grätzel, M. Sequential Deposition as a Route to High-Performance Perovskite-Sensitized Solar Cells. *Nature* **2013**, *499*, 316−319.

(17) Chen, Q.; Zhou, H.; Hong, Z.; Luo, S.; Duan, H.-S.; Wang, H.-H.; Liu, Y.; Li, G.; Yang, Y. Planar Heterojunction Perovskite Solar Cells via Vapor-Assisted Solution Process. *J. Am. Chem. Soc.* **2014**, *136*, 622−625.

(18) Yang, J.; Chen, S.; Xu, J.; Zhang, Q.; Liu, H.; Liu, Z.; Yuan, M. A Review on Improving the Quality of Perovskite Films in Perovskite Solar Cells via the Weak Forces Induced by Additives. *Appl. Sci.* **2019**, *9*, 4393.

(19) Li, H.; Wu, G.; Li, W.; Zhang, Y.; Liu, Z.; Wang, D.; Liu, S.; Frank. Additive Engineering to Grow Micron-Sized Grains for Stable High Efficiency Perovskite Solar Cells. *Adv. Sci.* **2019**, *6*, 1901241.

(20) Zhang, F.; Zhu, K. Additive Engineering for Efficient and Stable Perovskite Solar Cells. *Adv. Energy Mater.* **2020**, *10*, 1902579.

(21) Liu, S.; Guan, Y.; Sheng, Y.; Hu, Y.; Rong, Y.; Mei, A.; Han, H. A Review on Additives for Halide Perovskite Solar Cells. *Adv. Energy Mater.* **2020**, *10*, 1902492.

(22) Sartorio, C.; Scaramuzza, S.; Cataldo, S.; Vetri, V.; Scopelliti, M.; Leone, M.; Amendola, V.; Pignataro, B. Donor−Acceptor Interfaces by Engineered Nanoparticles Assemblies for Enhanced Efficiency in Plastic Planar Heterojunction Solar Cells. *J. Phys. Chem. C* **2016**, *120*, 26588−26599.

(23) Sartorio, C.; Campisciano, V.; Chiappara, C.; Cataldo, S.; Scopelliti, M.; Gruttadauria, M.; Giacalone, F.; Pignataro, B. Enhanced Power-Conversion Efficiency in Organic Solar Cells Incorporating Copolymeric Phase-Separation Modulators. *J. Mater. Chem. A* **2018**, *6*, 3884−3894.

(24) Bonasera, A.; Giuliano, G.; Arrabito, G.; Pignataro, B. Tackling Performance Challenges in Organic Photovoltaics: An Overview about Compatibilizers. *Molecules* **2020**, *25*, 2200.

(25) Ahmad, T.; Wilk, B.; Radicchi, E.; Fuentes Pineda, R.; Spinelli, P.; Herterich, J.; Castriotta, L. A.; Dasgupta, S.; Mosconi, E.; De Angelis, F.; Kohlstädt, M.; Würfel, U.; Di Carlo, A.; Wojciechowski, K. New Fullerene Derivative as an N-Type Material for Highly Efficient, Flexible Perovskite Solar Cells of a p-i-n Configuration. *Adv. Funct. Mater.* **2020**, *30*, 2004357.

(26) Zhang, W.; Pathak, S.; Sakai, N.; Stergiopoulos, T.; Nayak, P. K.; Noel, N. K.; Haghighirad, A. A.; Burlakov, V. M.; deQuilettes, D. W.; Sadhanala, A.; Li, W.; Wang, L.; Ginger, D. S.; Friend, R. H.; Snaith, H. J. Enhanced Optoelectronic Quality of Perovskite Thin Films with Hypophosphorous Acid for Planar Heterojunction Solar Cells. *Nat. Commun.* **2015**, *6*, 10030.

(27) Li, G.; Zhang, T.; Zhao, Y. Hydrochloric Acid Accelerated Formation of Planar CH3NH3PbI3 Perovskite with High Humidity Tolerance. *J. Mater. Chem. A* **2015**, *3*, 19674−19678.

(28) Chen, P.; Zhang, Y.; Du, J.; Wang, Y.; Zhang, X.; Liu, Y. Global Control of CH3NH3PbI3 Formation with Multifunctional Ionic Liquid for Perovskite Hybrid Photovoltaics. *J. Phys. Chem. C* **2018**, *122*, 10699−10705.

(29) Xia, R.; Gao, X. X.; Zhang, Y.; Drigo, N.; Queloz, V. I. E.; Tirani, F. F.; Scopelliti, R.; Huang, Z.; Fang, X.; Kinge, S.; Fei, Z.; Roldán-Carmona, C.; Nazeeruddin, M. K.; Dyson, P. J. An Efficient Approach to Fabricate Air-Stable Perovskite Solar Cells via Addition of a Self-Polymerizing Ionic Liquid. *Adv. Mater.* **2020**, *32*, 2003801.
(30) Han, L.; Cong, S.; Yang, H.; Lou, Y.; Wang, H.; Huang, J.; Zhu, J.; Wu, Y.; Chen, Q.; Zhang, B.; Zhang, L.; Zou, G. Environmental-Friendly Urea Additive Induced Large Perovskite Grains for High Performance Inverted Solar Cells. *Sol. RRL* **2018**, *2*, 1800054.
(31) Fu, J.; Sun, K.; Yang, K.; Hu, L.; Leng, C.; Kan, Z.; Duan, T.; Li, M.; Shi, H.; Xiao, Z.; Lu, S.; Ouyang, J. Efficiency Improvement of Planar Perovskite Solar Cells Using a Phenol Additive. *J. Mater. Chem. C* **2018**, *6*, 11519−11524.
(32) Liu, X.; Wu, J.; Guo, Q.; Yang, Y.; Luo, H.; Liu, Q.; Wang, X.; He, X.; Huang, M.; Lan, Z. Pyrrole: An Additive for Improving the Efficiency and Stability of Perovskite Solar Cells. *J. Mater. Chem. A* **2019**, *7*, 11764−11770.
(33) Hailegnaw, B.; Adam, G.; Wielend, D.; Pedarnig, J. D.; Sariciftci, N. S.; Scharber, M. C. Acetylacetone Improves the Performance of Mixed Halide Perovskite Solar Cells. *J. Phys. Chem. C* **2019**, *123*, 23807−23816.
(34) Guan, L.; Jiao, N.; Guo, Y. Trap-State Passivation by Nonvolatile Small Molecules with Carboxylic Acid Groups for Efficient Planar Perovskite Solar Cells. *J. Phys. Chem. C* **2019**, *123*, 14223−14228.
(35) Zhang, Z.; Fan, W.; Wei, X.; Zhang, L.; Yang, Z.; Wei, Z.; Shen, T.; Si, H.; Qi, J. Promoted Performance of Carbon Based Perovskite Solar Cells by Environmentally Friendly Additives of CH_3COONH_4 and $Zn(CH_3COO)_2$. *J. Alloys Compd.* **2019**, *802*, 694−703.
(36) Chang, C.-Y.; Chu, C.-Y.; Huang, Y.-C.; Huang, C.-W.; Chang, S.-Y.; Chen, C.-A.; Chao, C.-Y.; Su, W.-F. Tuning Perovskite Morphology by Polymer Additive for High Efficiency Solar Cell. *ACS Appl. Mater. Interfaces* **2015**, *7*, 4955−4961.
(37) Zhao, Y.; Wei, J.; Li, H.; Yan, Y.; Zhou, W.; Yu, D.; Zhao, Q. A Polymer Scaffold for Self-Healing Perovskite Solar Cells. *Nat. Commun.* **2016**, *7*, 10228.
(38) Yu, Y.-Y.; Tseng, C.; Chien, W.-C.; Hsu, H.-L.; Chen, C.-P. Photovoltaic Performance Enhancement of Perovskite Solar Cells Using Polyimide and Polyamic Acid as Additives. *J. Phys. Chem. C* **2019**, *123*, 23826−23833.
(39) Choi, M.-J.; Lee, Y.-S.; Cho, I. H.; Kim, S.; Kim, D.-H.; Kwon, S.-N.; Na, S.-I. Functional Additives for High-Performance Inverted Planar Perovskite Solar Cells with Exceeding 20% Efficiency: Selective Complexation of Organic Cations in Precursors. *Nano Energy* **2020**, *71*, 104639.
(40) Shargaieva, O.; Näsström, H.; Smith, J. A.; Többens, D.; Munir, R.; Unger, E. Hybrid Perovskite Crystallization from Binary Solvent Mixtures: Interplay of Evaporation Rate and Binding Strength of Solvents. *Mater. Adv.* **2020**, *1*, 3314.
(41) Hamill, J. C.; Schwartz, J.; Loo, Y.-L. Influence of Solvent Coordination on Hybrid Organic−Inorganic Perovskite Formation. *ACS Energy Lett.* **2018**, *3*, 92−97.
(42) Singh, S.; Kabra, D. Influence of Solvent Additive on the Chemical and Electronic Environment of Wide Bandgap Perovskite Thin Films. *J. Mater. Chem. C* **2018**, *6*, 12052−12061.
(43) Cao, X.; Zhi, L.; Jia, Y.; Li, Y.; Zhao, K.; Cui, X.; Ci, L.; Zhuang, D.; Wei, J. A Review of the Role of Solvents in Formation of High-Quality Solution-Processed Perovskite Films. *ACS Appl. Mater. Interfaces* **2019**, *11*, 7639−7654.
(44) Hussein, H. T.; Zamel, R. S.; Mohamed, M. S.; Mohammed, M. K. A. High-Performance Fully-Ambient Air Processed Perovskite Solar Cells Using Solvent Additive. *J. Phys. Chem. Solids* **2021**, *149*, 109792.
(45) Liang, P.-W.; Liao, C.-Y.; Chueh, C.-C.; Zuo, F.; Williams, S. T.; Xin, X.-K.; Lin, J.; Jen, A. K.-Y. Additive Enhanced Crystallization of Solution-Processed Perovskite for Highly Efficient Planar-Heterojunction Solar Cells. *Adv. Mater.* **2014**, *26*, 3748−3754.
(46) Tsai, C.-H.; Lin, C.-M.; Kuei, C.-H. Improving the Performance of Perovskite Solar Cells by Adding 1,8-Diiodooctane in the $CH_3NH_3PbI_3$ Perovskite Layer. *Sol. Energy* **2018**, *176*, 178−185.
(47) Peng, L.; Xie, W.; Yang, C. Study of the Effect of DIO Additive on Charge Extraction and Recombination in Organic−Inorganic Hybrid $MAPbI_{3-x}Cl_x$ Perovskite Solar Cell. *RSC Adv.* **2018**, *8*, 40298−40307.
(48) Cao, X.; Li, C.; Li, Y.; Fang, F.; Cui, X.; Yao, Y.; Wei, J. Enhanced Performance of Perovskite Solar Cells by Modulating the Lewis Acid−Base Reaction. *Nanoscale* **2016**, *8*, 19804−19810.
(49) Cao, X.; Zhi, L.; Li, Y.; Fang, F.; Cui, X.; Yao, Y.; Ci, L.; Ding, K.; Wei, J. Elucidating the Key Role of a Lewis Base Solvent in the Formation of Perovskite Films Fabricated from the Lewis Adduct Approach. *ACS Appl. Mater. Interfaces* **2017**, *9*, 32868−32875.
(50) Cao, X. B.; Li, C. L.; Zhi, L. L.; Li, Y. H.; Cui, X.; Yao, Y. W.; Ci, L. J.; Wei, J. Q. Fabrication of High Quality Perovskite Films by Modulating the Pb−O Bonds in Lewis Acid−Base Adducts. *J. Mater. Chem. A* **2017**, *5*, 8416−8422.
(51) Zhang, Y.; Gao, P.; Oveisi, E.; Lee, Y.; Jeangros, Q.; Grancini, G.; Paek, S.; Feng, Y.; Nazeeruddin, M. K. PbI_2−HMPA Complex Pretreatment for Highly Reproducible and Efficient $CH_3NH_3PbI_3$ Perovskite Solar Cells. *J. Am. Chem. Soc.* **2016**, *138*, 14380−14387.
(52) Hamill, J. C.; Romiluyi, O.; Thomas, S. A.; Cetola, J.; Schwartz, J.; Toney, M. F.; Clancy, P.; Loo, Y.-L. Sulfur-Donor Solvents Strongly Coordinate Pb^{2+} in Hybrid Organic−Inorganic Perovskite Precursor Solutionsr. *J. Phys. Chem. C* **2020**, *124*, 14496−14502.
(53) Zhi, L.; Li, Y.; Cao, X.; Li, Y.; Cui, X.; Ci, L.; Wei, J. Perovskite Solar Cells Fabricated by Using an Environmental Friendly Aprotic Polar Additive of 1,3-Dimethyl-2-Imidazolidinone. *Nanoscale Res. Lett.* **2017**, *12*, 632.
(54) Sales, A.; Felipe, L. d. O.; Bicas, J. L. Production, Properties, and Applications of α-Terpineol. *Food Bioprocess Technol.* **2020**, *13*, 1261−1279.
(55) Jones, E. W.; Holliman, P. J.; Connell, A.; Davies, M. L.; Baker, J.; Hobbs, R. J.; Ghosh, S.; Furnell, L.; Anthony, R.; Pleydell-Pearce, C. A Novel Dimethylformamide (DMF) Free Bar-Cast Method to Deposit Organolead Perovskite Thin Films with Improved Stability. *Chem. Commun.* **2016**, *52*, 4301−4304.
(56) Guo, X.; McCleese, C.; Gao, W.; Wang, M.; Sang, L.; Burda, C. Investigation of Moisture Stability and PL Characteristics of Terpineol-Passivated Organic−Inorganic Hybrid Perovskite. *Mater. Renew. Sustain. Energy* **2016**, *5*, 17.
(57) Acik, M.; Alam, T. M.; Guo, F.; Ren, Y.; Lee, B.; Rosenberg, R. A.; Mitchell, J. F.; Park, I. K.; Lee, G.; Darling, S. B. Substitutional Growth of Methylammonium Lead Iodide Perovskites in Alcohols. *Adv. Energy Mater.* **2018**, *8*, 1701726.
(58) Ghosh, S.; Mishra, S.; Singh, T. Antisolvents in Perovskite Solar Cells: Importance, Issues, and Alternatives. *Adv. Mater. Interfaces* **2020**, *7*, 2000950.
(59) Wu, J.; Zhang, W.; Wang, Q.; Liu, S.; Du, J.; Mei, A.; Rong, Y.; Hu, Y.; Han, H. A Favored Crystal Orientation for Efficient Printable Mesoscopic Perovskite Solar Cells. *J. Mater. Chem. A* **2020**, *8*, 11148−11154.
(60) Glaser, T.; Müller, C.; Sendner, M.; Krekeler, C.; Semonin, O. E.; Hull, T. D.; Yaffe, O.; Owen, J. S.; Kowalsky, W.; Pucci, A.; Lovrinčić, R. Infrared Spectroscopic Study of Vibrational Modes in Methylammonium Lead Halide Perovskites. *J. Phys. Chem. Lett.* **2015**, *6*, 2913−2918.
(61) Patel, J. B.; Milot, R. L.; Wright, A. D.; Herz, L. M.; Johnston, M. B. Formation Dynamics of $CH_3NH_3PbI_3$ Perovskite Following Two-Step Layer Deposition. *J. Phys. Chem. Lett.* **2016**, *7*, 96−102.
(62) Zhu, Z.; Hadjiev, V. G.; Rong, Y.; Guo, R.; Cao, B.; Tang, Z.; Qin, F.; Li, Y.; Wang, Y.; Hao, F.; Venkatesan, S.; Li, W.; Baldelli, S.; Guloy, A. M.; Fang, H.; Hu, Y.; Yao, Y.; Wang, Z.; Bao, J. Interaction of Organic Cation with Water Molecule in Perovskite $MAPbI_3$: From Dynamic Orientational Disorder to Hydrogen Bonding. *Chem. Mater.* **2016**, *28*, 7385−7393.
(63) Kato, Y.; Ono, L. K.; Lee, M. V.; Wang, S.; Raga, S. R.; Qi, Y. Silver Iodide Formation in Methyl Ammonium Lead Iodide

Perovskite Solar Cells with Silver Top Electrodes. *Adv. Mater. Interfaces* **2015**, *2*, 1500195.
(64) Uhl, A. R. Metal Counter Electrodes for Perovskite Solar Cells. *Counter Electrodes for Dye-Sensitized and Perovskite Solar Cells*; John Wiley & Sons, Ltd., 2018; pp 421−456.
(65) Yang, Y.; Wu, J.; Wang, X.; Guo, Q.; Liu, X.; Sun, W.; Wei, Y.; Huang, Y.; Lan, Z.; Huang, M.; Lin, J.; Chen, H.; Wei, Z. Suppressing Vacancy Defects and Grain Boundaries via Ostwald Ripening for High-Performance and Stable Perovskite Solar Cells. *Adv. Mater.* **2020**, *32*, 1904347.

https://doi.org/10.1021/acsaelm.1c00084
ACS Appl. Electron. Mater. 2021, 3, 1813−1825